IEEE Access
Multidisciplinary | Rapid Review | Open Access Journal

Received 14 September 2022, accepted 29 October 2022, date of publication 7 November 2022, date of current version 14 November 2022.

Digital Object Identifier 10.1109/ACCESS.2022.3220365

RESEARCH ARTICLE

Recognition of Key Information in Non-Stationary Signals Based on Wavelet Threshold Denoising and Back Propagation Neural Network Optimized by Manta Ray Foraging Optimization Algorithm

FUJING XU, TINGWEI JIA, AND RUIRUI JING
School of Automation and Software Engineering, Shanxi University, Taiyuan 030013, China
Corresponding author: Fujing Xu (xufujing@126.com)

This work was supported by the National Natural Science Foundation of China under Grant 61903240.

ABSTRACT The identification of key information hidden in non-stationary signals is challenging in various fields such as logistics and transportation, biomedicine, and fault diagnosis. To facilitate this identification, we propose a back propagation neural network (BPNN) recognition algorithm based on wavelet threshold denoising (WTD) and manta ray foraging optimization (MRFO) algorithm for the first time. The algorithm first performs WTD on the original signals, which can better extract features of the original signals. Subsequently, in order to improve the convergence speed of recognition model, MRFO algorithm is used to optimize the initial weights and thresholds of BPNN. On the base of this, the optimization model is finally obtained to recognize the key information in non-stationary signals. The comparative experimental results indicate that the proposed WTD-MRFO-BPNN algorithm has higher performance in key information recognition. The recognition accuracy reaches 97.25%.

INDEX TERMS Non-stationary signals, key information recognition, WTD, MRFO, BPNN.

I. INTRODUCTION

Non-stationary signals are utilized in many fields such as logistics and transportation safety, biomedical signal analysis, fault diagnosis, and geological exploration. In addition, these non-stationary signals contain lots of key information which is vital for biomedical signal analysis and fault diagnosis. To accurately recognize the key information, non-stationary signals are typically required to be denoised. Conventional denoising methods use low-pass filters [1], [2], [3], which facilitate denoising by blocking the high-frequency regions of signals. However, a low-pass filter cannot selectively allow significant information in the high frequency region to pass. To overcome the limitation of conventional denoising method, some other methods have been proposed, such as WTD, singular value decomposition (SVD) denoising, and empirical mode decomposition (EMD) denoising. SVD [4], [5], [6], [7], [8] is a nonlinear and non-stationary signal processing method and provides efficient denoising. But when detecting key information in a strong noise background, it cannot achieve an ideal denoising effect. EMD [9], [10], [11], [12] is a signal decomposition and denoising method. In practice, due to problems such as mode mixing and endpoint effect, the application of EMD is limited. WTD [13], [14] is relatively easy to perform and has a high noise reduction effect. Therefore, WTD method has been widely applied for denoising.

Of the key information in non-stationary signals, the most representative components are the shock features hidden in vibration signals. Currently, the recognition of the shock feature is performed by the method of moving crest factor and threshold. Zhou et al. [15] employed the moving crest factor and one-tenth peak value method to distinguish between the vibration and shock in vehicle vibration signals. This method is sensitive to window lengths. Selecting excessively large window lengths can cause the shock feature in the signals to

The associate editor coordinating the review of this manuscript and approving it for publication was Hongli Dong.

be masked, while selecting excessively small window lengths can easily lead to misrecognition. With the advancements in research on machine learning and deep learning, algorithms such as support vector machine (SVM) and artificial neural network have been extensively applied for the recognition of key information in non-stationary signals. Shao et al. [16] used SVM for fault diagnosis in rolling bearings. Although SVM can handle datasets with large sample sizes, it is sensitive to data and prone to overfitting. As a typical artificial neural network, BPNN [17], [18], [19], [20], [21], [22], [23], [24], [25] has been extensively used for mechanical fault diagnosis because of its superior nonlinear mapping ability. Nevertheless, typically, training parameters for the BPNN model are randomly selected. If the initial weights and thresholds are not selected appropriately, the BPNN will be constrained to a local extreme value. Zhang et al. [25] presented a fault diagnosis method based on BPNN optimized by particle swarm optimization (PSO) algorithm and applied the model for the fault diagnosis of plunger pump hydraulic system. However, the speed of the PSO algorithm cannot be adjusted dynamically. Thus, the PSO algorithm is facile to fall into local optimum. Therefore, it is not possible to consistently obtain improved results after every iteration.

It is vital for engineering fields to accurately identify key information. Unfortunately, the existing key information recognition methods cannot meet the requirements of effective recognition. Due to the excellent application of MRFO in global optimization problems [26], [27], a method is proposed in this study to identify key information using WTD denoising and MRFO-BPNN recognition algorithm. The WTD algorithm is used to denoise non-stationary signals, facilitating the extraction and construction of feature vectors with more prominent key information. Then the MRFO algorithm is employed to optimize the initial training parameters of BPNN. Finally, the WTD-MRFO-BPNN recognition model is obtained, which is used to identify the critical shock feature hidden in non-stationary signals.

The main contributions of this study are as follows:

(1) The WTD algorithm is used to denoise non-stationary signals before training BPNN to improve the recognition accuracy of key information.

(2) The moving-root-mean-square feature, moving-kurtosis feature, and upper-envelope feature are extracted from the denoised signals as predictors, and the MRFO algorithm is used to solve the problem that the initial parameters of BPNN are randomly determined.

(3) The experimental results show that WTD-MRFO-BPNN provides the best classification and recognition performance compared with WTD-PSO-BPNN, WTD-WOA-BPNN, PSO-BPNN, MRFO-BPNN and WOA-BPNN.

II. RELATED WORKS

A. WTD ALGORITHM

In non-stationary signals, significant information is typically contained in the low-frequency bands, whereas the high-frequency bands contain more detailed information and noise. In order to filter out the noise in non-stationary signals, different wavelet coefficients of the important information and noise can be used to establish a threshold function for threshold processing.

Hard threshold function and soft threshold function are traditional wavelet threshold functions. The hard threshold function can cause Gibbs effect after signal denoising. Thus, the soft threshold function is used in this study to denoise the non-stationary signals. Formula (1) represents the soft threshold function.

$$\omega_{thr} = \begin{cases} [sign(\omega)]\,(|\omega| - thr)\,, & |\omega| \geq thr \\ 0, & |\omega| < thr \end{cases} \tag{1}$$

where ω is the wavelet coefficient, ω_{thr} is the wavelet coefficient after applying the threshold, and thr is the threshold.

The entire denoising process is shown in Figure 1. The steps involved in the process are as follows.

(1) Determine the mother wavelet function and wavelet decomposition level, and decompose the noisy signal with the Mallat algorithm to get the corresponding high-frequency and low-frequency coefficients.

(2) Select an appropriate threshold function, perform threshold processing on the high-frequency coefficients after wavelet decomposition, and ensure that the low-frequency coefficients are unchanged.

(3) Reconstruct the signal using the low-frequency and high-frequency coefficients obtained after threshold processing.

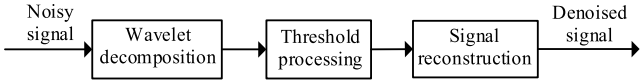

FIGURE 1. WTD process.

For 1D signals, three layers of decomposition layers are considered. Figure 2 shows the detailed process of wavelet decomposition and reconstruction, where CA_i represents the low-frequency part and CD_i represents the high-frequency part, with $i = 1, 2, 3$.

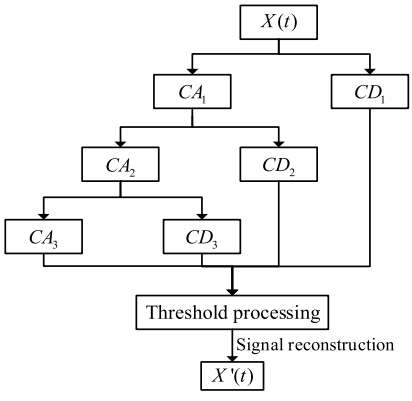

FIGURE 2. Wavelet decomposition and reconstruction process.

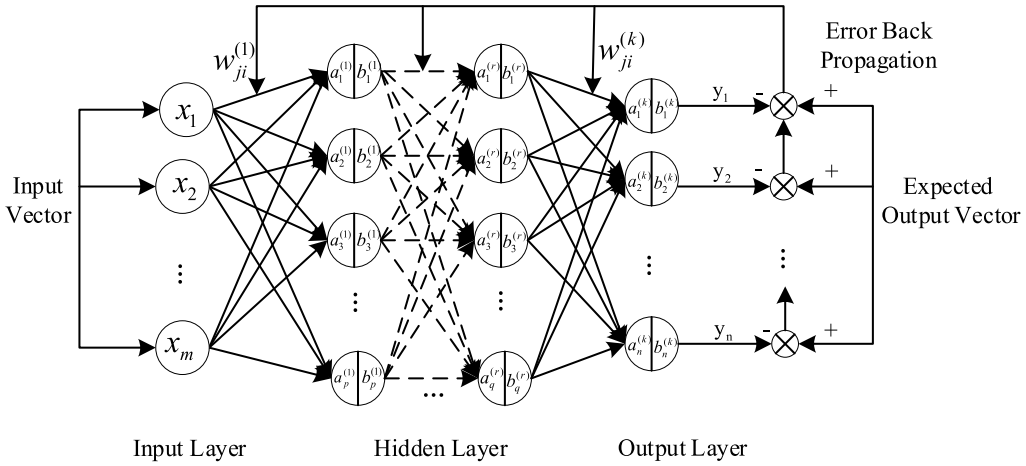

FIGURE 3. Basic structure diagram of BPNN.

B. BPNN ALGORITHM

BPNN is an algorithm that simulates the structure of the human nervous system. The learning process of BPNN involves the forward transfer of information and backpropagation of error. By continuously adjusting the connection weights and thresholds between layers, the sum of squared error in the output layer of the network is minimized, and an optimal neural network model for information recognition is obtained. The basic structure of BPNN is shown in Figure 3.

The BPNN is composed of several nodes, and each node represents a neuron. The j-th node of the l-th layer is denoted as A_j, and its input is:

$$a_j^{(l)} = \sum_{i=1}^{h} w_{ji} \cdot o_i \tag{2}$$

where o_i is the output of the i-th neuron in the previous layer; w_{ji} is the connection weight between the i-th neuron in the previous layer and the neuron A_j; h is the number of neurons in the previous layer. $b_j^{(l)}$ is the threshold of A_j. Then the output of A_j is:

$$y_j^{(l)} = f\left(a_j^{(l)}\right) + b_j^l \tag{3}$$

where $f(\cdot)$ is the activation function, due to which the output signal has a close resemblance to the signal in biological neurons.

C. MRFO ALGORITHM

The MRFO algorithm [28] is an intelligent optimization algorithm to simulate the foraging process of manta rays. MRFO involves three position update methods corresponding to three types of foraging behaviors: chain foraging, cyclone foraging and somersault foraging.

1) CHAIN FORAGING

Manta ray populations are linked head-to-tail in an orderly predation chain. The current optimal solution and the previous individual position of the individual manta ray are used to determine the moving direction and step size of the next individual position. The corresponding mathematical model is described as follows:

$$x_i^d(t+1) = \begin{cases} x_i^d(t) + r\left(x_{best}^d(t) - x_i^d(t)\right) + \alpha\left(x_{best}^d(t) - x_i^d(t)\right) \\ \qquad i = 1 \\ x_i^d(t) + r\left(x_{i-1}^d(t) - x_i^d(t)\right) + \alpha\left(x_{best}^d(t) - x_i^d(t)\right) \\ \qquad i = 2, 3, \cdots, N \end{cases} \tag{4}$$

$$\alpha = 2r\sqrt{|\log(r)|} \tag{5}$$

where $x_i^d(t)$ represents the position of the t-th generation and i-th individual on the d-th dimension; r represents a random vector in the interval of [0,1]; $x_{best}^d(t)$ represents the position of the t-th generation optimal individual on the d-th dimension; N represents the population size; α represents the weight coefficient.

2) CYCLONE FORAGING

Upon finding a prey, individual manta ray approach it in a spiral fashion. And each manta ray is affected by the manta ray preceding it in the spiral foraging progress. The corresponding mathematical model is described as follows:

When $\frac{t}{T} \geq rand$,

$$x_i^d(t+1) = \begin{cases} x_{best}^d + r\left(x_{best}^d(t) - x_i^d(t)\right) + \beta\left(x_{best}^d(t) - x_i^d(t)\right) \\ \qquad i = 1 \\ x_{best}^d + r\left(x_{i-1}^d(t) - x_i^d(t)\right) + \beta\left(x_{best}^d(t) - x_i^d(t)\right) \\ \qquad i = 2, 3, \cdots, N \end{cases} \tag{6}$$

$$\beta = 2e^{r_1 \frac{T-t+1}{T}} \sin(2\pi r_1) \tag{7}$$

where T represents the maximum number of iterations; r_1 represents a random number in [0,1]; β represents a weight coefficient.

When $\frac{t}{T} < rand$,

$$x_i^d(t+1) = \begin{cases} x_{rand}^d + r\left(x_{rand}^d - x_i^d(t)\right) + \beta\left(x_{rand}^d - x_i^d(t)\right) \\ \qquad i = 1 \\ x_{rand}^d + r\left(x_{i-1}^d(t) - x_i^d(t)\right) + \beta\left(x_{rand}^d - x_i^d(t)\right) \\ \qquad i = 2, 3, \cdots, N \end{cases} \tag{8}$$

$$x_{rand}^d = Lb^d + r\left(Ub^d - Lb^d\right) \tag{9}$$

where x_{rand}^d represents a random position on the d-th dimension. Ub^d and Lb^d represent the upper and lower bounds of the variable.

3) SOMERASAULT FORAGING

In somersault foraging, each manta ray somersaults around the prey's position and falls to a new position. The corresponding mathematical model is described as follows:

$$x_i^d(t+1) = x_i^d(t) + S\left(r_2 x_{best}^d - r_3 x_i^d(t)\right), \quad i = 1, 2, \cdots, N \tag{10}$$

where S is the somersault factor with a value of 2; r_2 and r_3 represent random numbers in [0,1].

III. FEATURE RECOGNITION METHOD BY WTD-MRFO-BPNN MODEL

This study intends to use the vibration acceleration signals during the driving process of the vehicle to simulate the relevant non-stationary signals and then recognize the key information (such as typical shock features). The flow chart of WTD-MRFO-BPNN model is shown in Figure 4. Since the vehicle vibration signals usually contain a lot of noise information, WTD is firstly used to denoise the noisy signals. Following this, a feature vector with significant shock features is constructed by extracting the moving-root-mean-square feature, moving-kurtosis feature, and upper-envelope feature of the denoised signal. To prevent BPNN from readily falling into the local extreme value caused by conventional initialization parameters, the MRFO algorithm is adopted, which optimizes the initial weights and thresholds of the BPNN. The recognition model can be obtained by introducing the optimization result into the BPNN. Finally, the feature vector is used as the input vector of the recognition model to recognize the shock.

A. WTD DENOISING

In this study, WTD is firstly performed on the vehicle vibration signals. Daubechies 8 (db8) wavelet is selected to decompose and reconstruct the vehicle vibration signals. The number of layers of wavelet decomposition can directly affect the degree of distortion of the reconstructed signal. Thus, as the number of decomposition layers increases, the difference between the noise and the real signal increases. Therefore, the number of decomposition layers is finally selected to be five. Moreover, MATLAB's own function (Formula (11)) is selected to obtain the threshold. The signal is processed by threshold function and then reconstructed to obtain the denoised signal.

$$thr = thselect(s, \text{'}heursure\text{'}) \tag{11}$$

where s is the signal to be denoised, and *heursure* is the heuristic threshold.

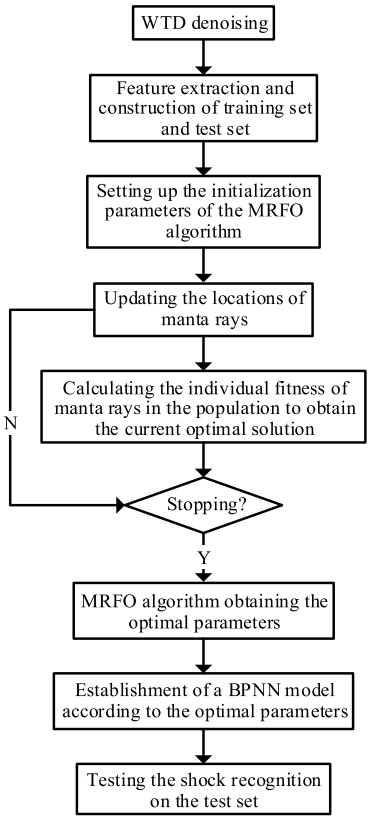

FIGURE 4. The flow chart of WTD-MRFO-BPNN model.

B. FEATURE VECTOR CONSTRUCTION

As the shock has the characteristics of high amplitude and short duration, we can obviously observe the characteristics of peak changes in the data by calculating the moving-root-mean-square feature, moving-kurtosis feature and upper-envelope feature. Therefore, this study extracts the features of the denoised signals from these three aspects, thereby obtaining relatively complete state information of the denoised signal. Feature vector is constructed through the extracted features.

The forward and backward moving-root-mean-square features are extracted for two different window lengths of 0.05s and 0.7s. Similarly, the forward and backward moving-kurtosis features are extracted for two different window lengths of 0.4s and 0.8s. Among the extracted features, the forward features use the current time point t_0 as the starting point and the window length T along the development

direction of the time axis to calculate the characteristics over the time period $t_0 + T$. The backward features are extracted in an opposite manner. The acquisition method of the upper-envelope feature is to find all the local extreme points in the signal at the absolute value of the signal. Then, according to these upper extreme points, the envelope curve is fitted by the cubic spline interpolation method, and the upper-envelope feature is generated by the envelope curve.

Formulas (12) and (13) show the calculation methods of moving-root-mean-square feature and moving-kurtosis feature. The forward and backward features lie in the integration intervals [0, T] and [-T, 0], respectively, where T is the length of the window.

$$m_{RMS}(t) = \sqrt{\frac{1}{T}\int_0^T x(t+\tau)^2 d\tau} \tag{12}$$

$$K(t) = \frac{\frac{1}{T}\int_0^T [x(t+\tau)]^4 d\tau}{\left(\frac{1}{T}\int_0^T [x(t+\tau)]^2 d\tau\right)^2} \tag{13}$$

C. MRFO-BPNN RECOGNITION MODEL

Although BPNN offers remarkable advantages in terms of error backpropagation and updating of weights and thresholds, the convergence direction of BPNN depends on initial weights and thresholds. The MRFO algorithm uses the mean-square error (MSE) of the predicted results with respect to the actual results in the training, setting as the fitness function, to iteratively generate the weights and thresholds of BPNN, and to establish a BPNN by the set of optimal weights and thresholds. This leads to the generation of a shock feature recognition model.

The process of optimizing BPNN using MRFO involves the following steps.

Step 1: Determine the topology of the BPNN, including the number of input neurons n_{in}, the number of output neurons n_{out}, the number of hidden layers k ($k = 3$ for this study), and the number of neurons n_i in each hidden layer with $i = 1$, 2, 3; n_{in} and n_{out} also denote the input and output dimensions of the network.

Step 2: Determine the corresponding relationship between the individual manta ray optimization position and the network weights and thresholds, that is, each dimension represents a weight or threshold. Calculate the dimension d of the optimization position. The calculation formula is shown below.

$$\begin{aligned} d = {} & n_{in} \times n_1 + n_1 + n_1 \times n_2 + n_2 \\ & + n_2 \times n_3 + n_3 + n_3 \times n_{out} + n_{out} \end{aligned} \tag{14}$$

where n_{in} and n_{out} are 9 and 1, respectively; n_1, n_2 and n_3 are 16, 10 and 5, respectively.

Step 3: Initialize other parameters of MRFO-BPNN including population size N, maximum number of iterations T, somersault factor S, and boundary values Ub and Lb of the optimization position.

Step 4: Determine the initial position randomly. Using the initial population to calculate the fitness value of manta rays.

Step 5: Determine whether the maximum number of iterations is reached. If so, go to **step 10**; otherwise, generate a random number *rand*.

Step 6: If *rand* < 0.5, go to **step 7**; otherwise, update the position according to formula (4) and calculate the individual fitness value.

Step 7: Judge whether t/T is less than *rand*. If it is, then update the position according to formula (8); otherwise, update the position according to formula (6) and calculate the individual fitness value.

Step 8: Compare whether the updated individual fitness value is less than the global individual fitness value. If so, use the new location to replace the global optimal location, otherwise keep the original global optimal location.

Step 9: Use formula (10) to update the location and calculate the individual fitness value. Evaluate the individual fitness and optimal location of the new generation population according to **step 8**. Then, return to **step 5**.

Step 10: Obtain the optimal position vector. Bring the optimization result into the BPNN for training. Use the test set to test the model recognition results.

IV. EXPERIMENT AND ANALYSIS

A. SIMULATION SIGNAL TEST

1) SIMULATION SIGNAL SYNTHESIS

The vibrations and shocks generated by the vehicle when driving are two different signals. Vibrations are non-stationary and are caused by factors such as vehicle speed and road-surface unevenness. Shocks are transient signals generated under abrupt conditions such as vehicle failure and sudden pavement change. Their duration is limited, and their amplitude changes significantly. Since vibrations and shocks are generated in different ways, they are simulated and synthesized separately. The synthesized vehicle vibration signal is generated by superposition.

The synthesis process of non-stationary vibration component involves four steps. First, the power spectral density (PSD) of the actual vehicle vibration signal can be used to obtain the required spectral shape. Then, the PSD data is adjusted by interpolation to meet the required sequence length. The signal is converted to the time domain through inverse fast Fourier transform, and a Gaussian random signal is obtained eventually. Afterwards, the amplitude modulation function is generated according to the root-mean-square value distribution function of the measured signal. Finally, the non-stationary vibration component is obtained by multiplying the Gaussian random signal by the modulation function. Figure 5 shows the result after the zero-mean normalization of the non-stationary vibration component. The zero-mean normalization formula is shown below.

$$x' = \frac{x - \bar{x}}{\sigma} \tag{15}$$

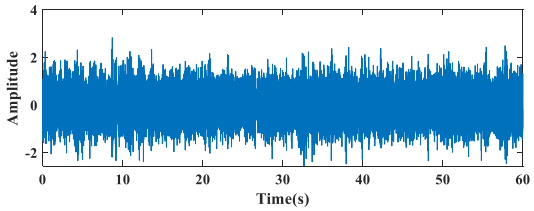

FIGURE 5. Non-stationary vibration component.

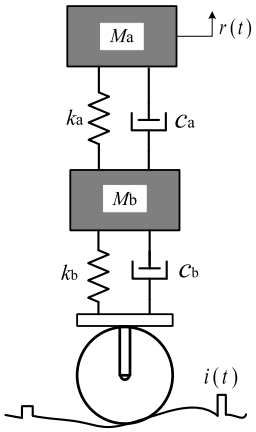

FIGURE 6. Two-degree-of-freedom car model.

TABLE 1. Parameter values of the two-degree-of-freedom car model.

Component	M_a	M_b	k_a	k_b	c_a	c_b
Value	8900 kg	1100 kg	2000 kN/m	3600 kN/m	40 kN s/m	4 kN s/m

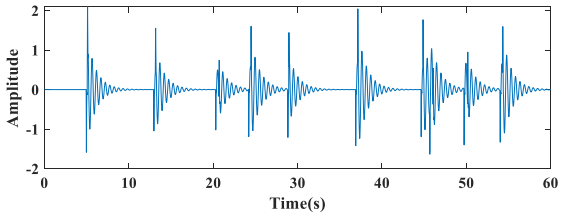

FIGURE 7. Shock component obtained by inputting the random pulse into the two-degree-of-freedom model.

where x is the original data, $\bar{x}$ and σ are the mean and standard deviation of the original data, respectively.

As shown in Figure 6, the quarter car model is used to synthesize the shock component. Table 1 [29] shows the value selected for each parameter. $i(t)$ represents a pulse function that simulates certain sudden conditions such as sudden pavement change and vehicle failure. The width and amplitude ranges of the pulse are selected to be [0.1s, 0.5s] and [10mm, 100mm], respectively. $r(t)$ represents the response to the random pulse, i.e., the shock component required to synthesize the vehicle vibration signal, as shown in Figure 7.

The obtained non-stationary vibration component is superimposed on the shock component to obtain the vehicle vibration acceleration simulation signal. Gaussian noise is introduced to the synthetic signal, and the signal-to-noise ratio is 10dBw, which makes the synthetic signal closer to the actual situation. Figure 8 shows the result after the zero-mean normalization of the signal. The position of the shock component is predetermined in the simulation process. The predetermined position information is conducive for model training and testing in later stage experiment.

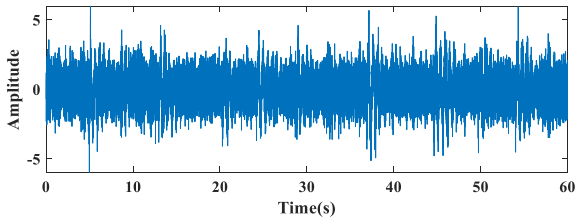

FIGURE 8. Synthetic non-stationary signal containing vibration and shock.

2) SHOCK RECOGNITION

The above method is employed to synthesize the non-stationary signal with 60s duration. The non-stationary signal is sampled at a rate of 1000 Hz. WTD and SVD denoising are applied to denoise the signal. The results are shown in Figure 9. It is observed that the WTD method has a more significant denoising effect.

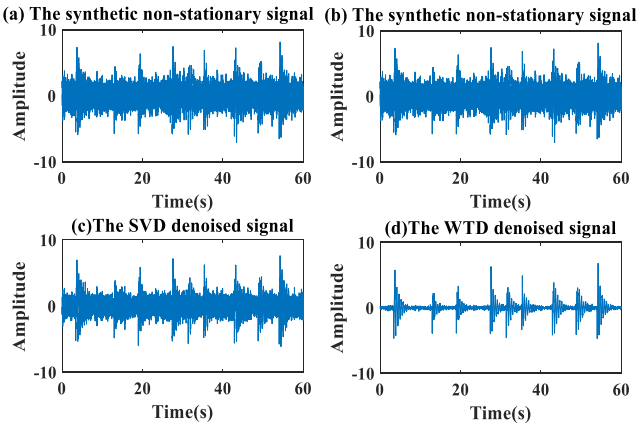

FIGURE 9. Comparison of denoising effects of WTD and SVD: (a) The synthetic non-stationary signal, (b) The synthetic non-stationary signal, (c) The SVD denoised signal and (d) The WTD denoised signal.

The local transient features are extracted from the denoised signal. The training and test sets are divided in a 2:1 ratio to conduct the model-optimization training. To verify the shock recognition effect of WTD-MRFO-BPNN algorithm presented in this study, WTD-MRFO-BPNN is compared with MRFO-BPNN, particle swarm optimization-back propagation neural network (PSO-BPNN), whale optimization algorithm-back propagation neural network

TABLE 2. Parameters settings in each optimization algorithm.

Algorithm	Parameters	Description	Value
MRFO	N	Manta ray population	20
	T	Maximum number of iterations	20
	S	The somersault factor	2
WOA	N	Whale population	20
	T	Maximum number of iterations	20
	a	Control parameter (Linely decreased over iteration)	2
	b	Constant coefficient	1
PSO	N	Particle swarm population	20
	T	Maximum number of iterations	20
	c_1, c_2	Learning factors	2

(WOA-BPNN), WTD-PSO-BPNN and WTD-WOA-BPNN. The basic parameters of these optimization algorithms are shown in Table 2. In each optimization model, the basic parameters of BPNN are the same. The initial weights and thresholds optimization interval of the BPNN is all $[-1, 1]$. When the activation functions of output layer and three hidden layers are 'purelin', 'logsig', 'logsig' and 'tansig', respectively, the classification and recognition effect of the model is the best. Additionally, the maximum training iterations, target error and learning rate are 1000, 0.001 and 0.1, respectively. Besides, the numbers of neurons in three hidden layers are 16, 10 and 5, respectively. The other related parameters of the BPNN are set to the default values. All algorithms are simulated using MATLAB 2018a, and the computer system has i5 core and 8.0 GB ram. The comparison diagram of the training process by different back propagation algorithms is shown in Figure 10.

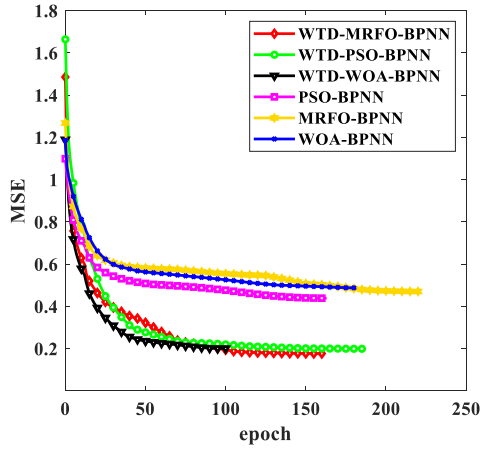

FIGURE 10. Comparison diagram of the training process by different BP algorithms.

The MSE is applied as the loss function of each recognition algorithm in Figure 10. As training proceeds, the MSE of all algorithms continuously decreases and converges. When the error curve is no longer continuously decreasing, the training is terminated to prevent overfitting of the network. Figure 10 shows that WTD-MRFO-BPNN, WTD-PSO-BPNN, WTD-WOA-BPNN, PSO-BPNN, MRFO-BPNN and WOA-BPNN have been trained for 162 epochs, 187 epochs, 102 epochs, 164 epochs, 221 epochs and 181 epochs, respectively. It can be observed that WTD-MRFO-BPNN has the best MSE (0.177).

The optimized recognition models are applied to recognize the test set. The recognition and comparison results of different algorithms are shown in Figure 11. In Figure 11, the TN region represents the correctly classified vibration; the FN region represents the misclassified shock; the TP region represents the correctly classified shock; the FP region represents the misclassified vibration. When the TP and TN regions account for a higher proportion, the classification and recognition effect of the obtained model is better. Figure 11 shows that the recognition effect using WTD-MRFO-BPNN is better than that using the other models, which can be attributed to accurate recognition of shock signals and a lower classification error rate.

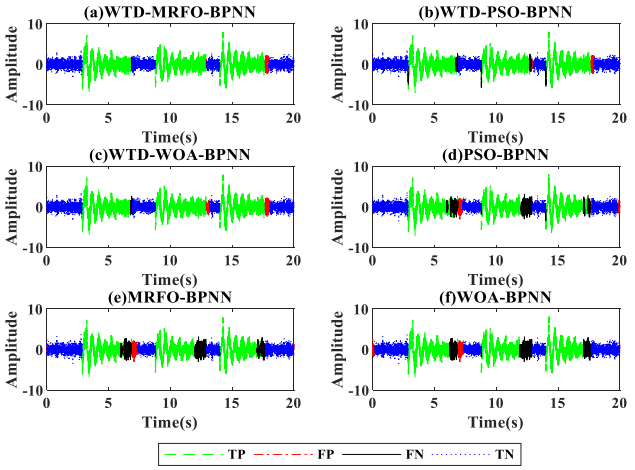

FIGURE 11. Shock recognition effects of test set using six recognition models: (a) WTD-MRFO-BPNN, (b) WTD-PSO-BPNN, (c) WTD-WOA-BPNN, (d) PSO-BPNN, (e)MRFO-BPNN and (f) WOA-BPNN.

The ROC curves of these recognition models are shown in Figure 12. The area under the ROC curve (AUC) of these recognition models in Figure 12 are 0.9977, 0.9967, 0.9964, 0.9535, 0.9597 and 0.9555, respectively. The closer AUC is to 1, the better the performance of the training recognition method is. Hence, WTD-MRFO-BPNN has better recognition performance.

To evaluate the recognition quality of each model more comprehensively, some indicators are introduced: recall rate (TPR), Matthews correlation coefficient (MCC), precision rate (Pr), F-measure (F1) and recognition accuracy (ACC). Formulas (16), (17), (18), (19) and (20) show the calculation methods adopted for each indicator. The comparison of the performance indicators for different algorithms is shown

TABLE 3. Comparison of the performance indicators for six recognition models.

Rate	AUC	TPR	MCC	Pr	F1	ACC
WTD-MRFO-BPNN	**0.9977**	**0.9653**	**0.9170**	**0.9636**	**0.9709**	**96.44%**
WTD-PSO-BPNN	0.9967	0.9430	0.8930	0.9595	0.9612	95.58%
WTD-WOA-BPNN	0.9964	0.9580	0.9083	0.9425	0.9573	95.04%
PSO-BPNN	0.9535	0.8160	0.7484	0.9561	0.8805	86.00%
MRFO-BPNN	0.9597	0.7968	0.7357	0.9536	0.8784	85.62%
WOA-BPNN	0.9555	0.8073	0.7319	0.9455	0.8738	85.78%

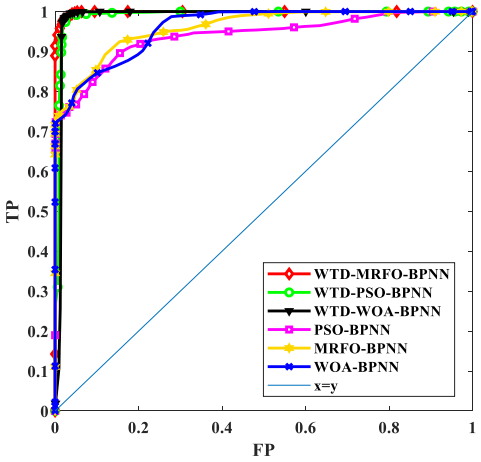

FIGURE 12. ROC curves using six recognition models.

in Table 3.

$$TPR = \frac{TP}{TP + FN} \tag{16}$$

$$MCC = \frac{(TP \times TN) - (FP \times FN)}{\sqrt{(TP+FN) \times (TP+FP) \times (TN+FN) \times (TN+FP)}} \tag{17}$$

$$Pr = \frac{TP}{TP + FP} \tag{18}$$

$$F1 = \frac{2 \times Pr \times TPR}{Pr + TPR} \tag{19}$$

$$ACC = \frac{TP + TN}{TP + TN + FP + FN} \tag{20}$$

Ideally, the closer TPR and Pr are to 1, the higher the classification accuracy of shock is. Similarly, the closer MCC and F1 are to 1, the better the recognition performance is. Note that the value range of MCC is [−1, 1]. Besides, the closer ACC is to 1, the higher the comprehensive recognition accuracy is. By comparing the data in Table 3, it can be concluded that the recognition result of WTD-MRFO-BPNN is superior to the other five models.

Confusion matrix for different recognition models is shown in Table 4. Each indicator in Table 4 reflects the performance of each recognition model. TP and TN (correct recognition rate) are expected to be extremely high, whereas FP and FN (false recognition rate) are expected to be extremely low. By comparing the six recognition models, it can be found that WTD-MRFO-BPNN has the optimal performance indicators.

TABLE 4. Confusion matrix using six recognition models (order: WTD-MRFO-BPNN/WTD-PSO-BPNN/WTD-WOA-BPNN/PSO-BPNN/MRFO-BPNN/WOA-BPNN).

Rate(%)		Predicted	
		1 (shock)	0 (vibration)
Actual	1 (shock)	**99.6**/97.3/98.8/81.7/ 79.1/80.7 (**TP**)	**0.4**/2.8/1.2/18.3/ 20.9/19.3 (**FN**)
	0 (vibration)	**3.6**/5.1/4.1/9.3/ 4.5/ 8.0 (**FP**)	**96.4**/92.0/95.5/94.9/ 95.9/90.6 (**TN**)

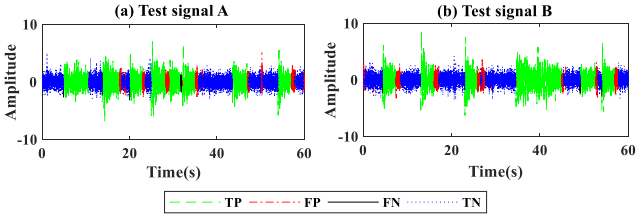

FIGURE 13. Classification and recognition results of test signals: (a) Test signal A, (b)Test signal B.

The trained model is adopted for shock recognition of the other two sets of non-stationary signals synthesized at the same parameter level. The recognition results are shown in Figure 13. The recognition results indicate that WTD-MRFO-BPNN has relatively good recognition ability.

B. ACTUAL SIGNAL TEST

To further verify the validity of the proposed method, it is applied to the vibration and shock recognition analysis of actual vehicle vibration signals, which are obtained by using a signal acquisition device fitted to a logistics transportation vehicle. The acquisition process is shown in Figure 14.

Figure 15(a) and Figure 15(b) are practically measured non-stationary signals after zero-mean normalization. The duration of the signal is 25s and its sampling frequency is 1000 Hz. Because the shock characteristic frequency is usually lower than the vibration characteristic frequency in non-stationary signals (such as vehicle vibration acceleration signals), the selected sampling frequency can present the entire features of the signal. The SVD is performed on the

TABLE 5. Comparison of performance indicators using different recognition models.

Rate	AUC	TPR	MCC	Pr	F1	ACC
WTD-MRFO-BPNN	**0.9993**	**0.9642**	**0.9695**	**0.9975**	**0.9709**	**97.25%**
WTD-PSO-BPNN	0.9967	0.9591	0.9153	0.9660	0.9373	96.69%
WTD-WOA-BPNN	0.9924	0.9526	0.9578	0.8591	0.9684	95.64%
PSO-BPNN	0.9857	0.8016	0.8542	0.9934	0.9474	95.52%
MRFO-BPNN	0.9557	0.8480	0.8770	0.9927	0.8944	95.30%
WOA-BPNN	0.9787	0.8818	0.8416	0.9949	0.9096	95.62%

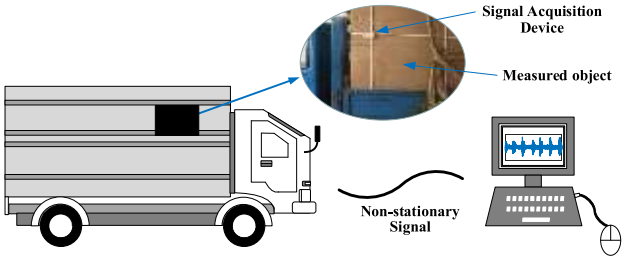

FIGURE 14. Actual signal acquisition process.

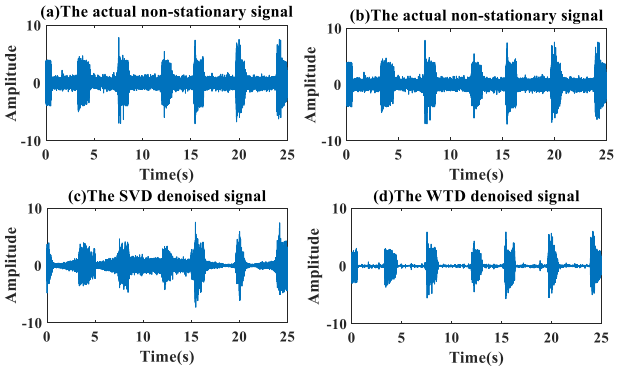

FIGURE 15. Comparison of denoising effects of WTD and SVD: (a) The actual non-stationary signal, (b) The actual non-stationary signal, (c) The SVD denoised signal and (d) The WTD denoised signal.

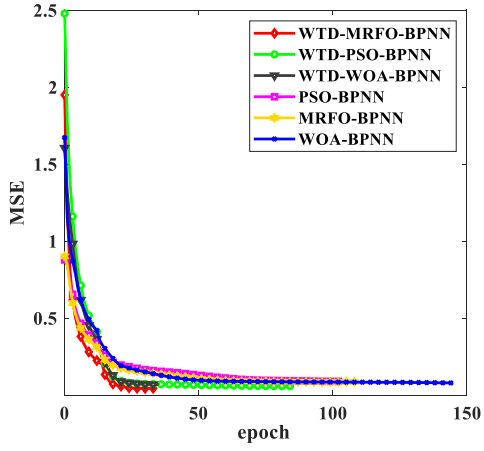

FIGURE 16. Comparison diagram of the training process by different BP algorithms.

actual signal, and the denoised signal is obtained, as shown in Figure 15(c). Compared with the SVD denoising method, the result of WTD denoising is shown in Figure 15(d).

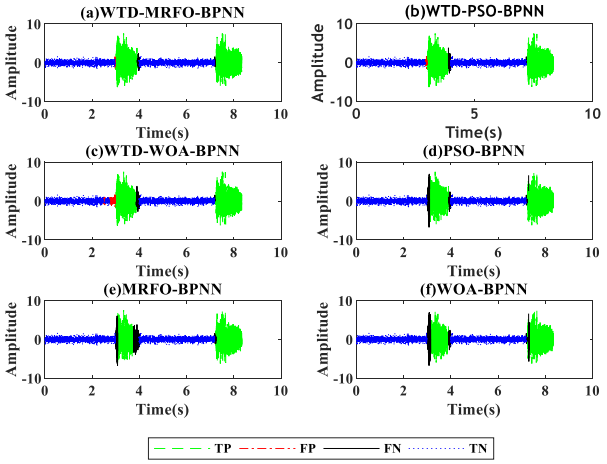

FIGURE 17. Shock recognition effects of actual signal using six recognition models: (a) WTD-MRFO-BPNN, (b) WTD-PSO-BPNN, (c) WTD-WOA-BPNN, (d) PSO-BPNN, (e)MRFO-BPNN and (f) WOA-BPNN.

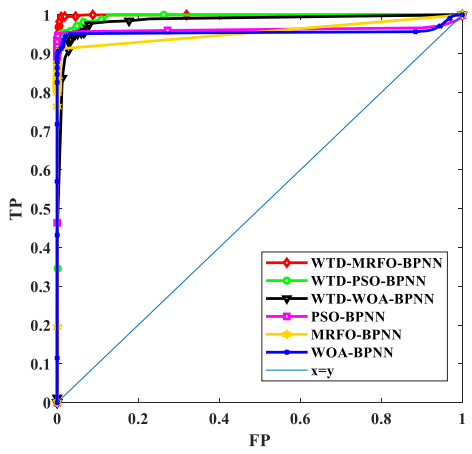

FIGURE 18. ROC curves of six recognition models.

The same method is employed for feature vector extraction and recognition model training of the measured signal. Subsequently, the dataset is divided in a ratio of training set: test set = 2:1. The parameters in each recognition algorithm are the same as before. The comparison diagram of the training process of different back propagation algorithms is shown in Figure 16. Figure 16 shows that WTD-MRFO-BPNN, WTD-PSO-BPNN, WTD-WOA-BPNN, PSO-BPNN, MRFO-BPNN and WOA-BPNN have

been trained for 34 epochs, 85 epochs, 36 epochs, 103 epochs, 109 epochs and 145 epochs, respectively. It is observed that WTD-MRFO-BPNN has better MSE (0.043) and training speed.

The test set is introduced to the trained recognition model for shock recognition. Figure 17 shows the recognition results using different recognition models. The recognition accuracy of the proposed model for the test set is 97.25%. The performance indicators of these six recognition models are compared, as shown in Table 5.

The ROC curves of these recognition models are shown in Figure 18. The AUC of these recognition models in Figure 18 are 0.9993, 0.9967, 0.9924, 0.9857, 0.9557 and 0.9787, respectively. Thus, WTD-MRFO-BPNN has better classification and recognition performance.

The above experimental results show that the WTD method can effectively retain the transient shock features of non-stationary signals when dealing with noisy signals. Furthermore, the MRFO optimization algorithm can avoid the characteristic of local optimum and make the classification result of the BPNN more ideal. Finally, by combining the WTD algorithm, MRFO algorithm and BPNN algorithm, a key information recognition model, which has a good recognition rate of shock and vibration in non-stationary signals, is obtained.

V. CONCLUSION

The recognition accuracy of key information in non-stationary signals is increasingly demanding in many research fields, such as logistics and transportation, biomedicine, and fault diagnosis. However, the problem of low recognition accuracy is common in traditional identification methods. Based on this, this study proposes a WTD-MRFO-BPNN key information recognition algorithm for the first time. For synthetic signals and collected signals, the proposed algorithm is compared with WTD-PSO-BPNN, WTD-WOA-BPNN, PSO-BPNN, MRFO-BPNN and WOA-BPNN. The recognition accuracy of the algorithm for the synthetic signal is up to 96.44%; the recognition accuracy of the actual collected signal can reach up to 97.25%, which are both higher than the other five methods. The results of the experiments indicate that the proposed WTD-MRFO-BPNN classification and recognition model has high accuracy and reliability.

At the same time, there are several limitations to this model: 1) the recognition accuracy of the model may be further improved. 2) the feature system of the model only considers the time domain feature. Therefore, future work will consider more features in other processing domains to enrich the feature system.

REFERENCES

[1] G. Bollati, S. Marchese, M. Demicheli, and R. Castello, "An eighth-order CMOS low-pass filter with 30–120 MHz tuning range and programmable boost," *IEEE J. Solid-State Circuits*, vol. 36, no. 7, pp. 1056–1066, Jul. 2001.

[2] G. L. Matthaei, "Tables of Chebyshev impedance–transforming networks of low-pass filter form," *Proc. IEEE*, vol. 52, no. 8, pp. 939–963, Aug. 1964.

[3] M. Tohidian, I. Madadi, and R. B. Staszewski, "Analysis and design of a high-order discrete-time passive IIR low-pass filter," *IEEE J. Solid-State Circuits*, vol. 49, no. 11, pp. 2575–2587, Nov. 2014.

[4] X. Cui, Z. Wang, Y. Kang, H. Pu, and Z. Deng, "A robust indicator based on singular value decomposition for flaw feature detection from noisy ultrasonic signals," *Meas. Sci. Technol.*, vol. 29, no. 5, Apr. 2018, Art. no. 055009.

[5] S. Gan, Y. Chen, S. Zu, S. Qu, and W. Zhong, "Structure-oriented singular value decomposition for random noise attenuation of seismic data," *J. Geophys. Eng.*, vol. 12, no. 2, pp. 262–272, 2015.

[6] A. Höcker and V. Kartvelishvili, "SVD approach to data unfolding," *Nucl. Instrum. Methods Phys. Res. A, Accel. Spectrom. Detect. Assoc. Equip.*, vol. 372, no. 3, pp. 469–481, Apr. 1996.

[7] Z. Qiao and Z. Pan, "SVD principle analysis and fault diagnosis for bearings based on the correlation coefficient," *Meas. Sci. Technol.*, vol. 26, no. 8, Jul. 2015, Art. no. 085014.

[8] D. Kalman, "A singularly valuable decomposition: The SVD of a matrix," *College Math. J.*, vol. 27, no. 1, pp. 2–23, 1996.

[9] A. O. Boudraa and J. C. Cexus, "EMD-based signal filtering," *IEEE Trans. Instrum. Meas.*, vol. 56, no. 6, pp. 2196–2202, Dec. 2007, doi: 10.1109/TIM.2007.907967.

[10] D. Yu, J. Cheng, and Y. Yang, "Application of EMD method and Hilbert spectrum to the fault diagnosis of roller bearings," *Mech. Syst. Signal Process.*, vol. 19, no. 2, pp. 259–270, Mar. 2005.

[11] Y. Lei, Z. He, and Y. Zi, "Application of the EEMD method to rotor fault diagnosis of rotating machinery," *Mech. Syst. Signal Process.*, vol. 23, no. 4, pp. 1327–1338, 2009.

[12] Y. Shrivastava and B. Singh, "A comparative study of EMD and EEMD approaches for identifying chatter frequency in CNC turning," *Eur. J. Mech., A/Solids*, vol. 73, pp. 381–393, Jan. 2019.

[13] W. Chen, J. Li, Q. Wang, and K. Han, "Fault feature extraction and diagnosis of rolling bearings based on wavelet thresholding denoising with CEEMDAN energy entropy and PSO-LSSVM," *Measurement*, vol. 172, Feb. 2021, Art. no. 108901.

[14] X. Xu, M. Luo, Z. Tan, and R. Pei, "Echo signal extraction method of laser radar based on improved singular value decomposition and wavelet threshold denoising," *Infr. Phys. Technol.*, vol. 92, pp. 327–335, Aug. 2018.

[15] H. Zhou and Z.-W. Wang, "A new approach for road-vehicle vibration simulation," *Packag. Technol. Sci.*, vol. 31, no. 5, pp. 246–260, May 2018.

[16] K. Shao, W. Fu, J. Tan, and K. Wang, "Coordinated approach fusing time-shift multiscale dispersion entropy and vibrational Harris hawks optimization-based SVM for fault diagnosis of rolling bearing," *Measurement*, vol. 173, Mar. 2021, Art. no. 108580.

[17] Z. Liu, Q. Tan, Y. Zhou, and H. Xu, "Syncretic application of IBAS-BP algorithm for monitoring equipment online in power system," *IEEE Access*, vol. 9, pp. 21769–21776, 2021.

[18] L. Wan, H. Li, G. Zhang, C. Li, J. Man, and M. Xiao, "Rolling bearing fault diagnosis method based on parallel QPSO-BPNN under spark-GPU platform," *IEEE Access*, vol. 9, pp. 56786–56801, 2021.

[19] J. Dong, W. Qin, and M. Wang, "Fast multi-objective optimization of multi-parameter antenna structures based on improved BPNN surrogate model," *IEEE Access*, vol. 7, pp. 77692–77701, 2019.

[20] C. Zhang, S. Yu, G. Li, and Y. Xu, "The recognition method of MQAM signals based on BP neural network and bird swarm algorithm," *IEEE Access*, vol. 9, pp. 36078–36086, 2021.

[21] H. Qin, R. Yang, C. Guo, and W. Wang, "Fault diagnosis of electric rudder system using PSOFOA-BP neural network," *Measurement*, vol. 186, Dec. 2021, Art. no. 110058.

[22] Y. Tian, J. Yu, and A. Zhao, "Predictive model of energy consumption for office building by using improved GWO-BP," *Energy Rep.*, vol. 6, pp. 620–627, Nov. 2020.

[23] B. Wang, X. Gu, L. Ma, and S. Yan, "Temperature error correction based on BP neural network in meteorological wireless sensor network," *Int. J. Sensor Netw.*, vol. 23, no. 4, pp. 265–278, Jan. 2017.

[24] Z. Zhao, Q. Xu, and M. Jia, "Improved shuffled frog leaping algorithm-based BP neural network and its application in bearing early fault diagnosis," *Neural Comput. Appl.*, vol. 27, no. 2, pp. 375–385, 2016.

[25] H. Zhang and L. Tao, "Application of PSO-BP algorithm in hydraulic system fault diagnosis," *J. Syst. Simul.*, vol. 28, no. 5, pp. 1186–1190, May 2016.
[26] A. Tang, H. Zhou, T. Han, and L. Xie, "A modified manta ray foraging optimization for global optimization problems," *IEEE Access*, vol. 9, pp. 128702–128721, 2021.
[27] G. Hu, M. Li, X. Wang, G. Wei, and C.-T. Chang, "An enhanced manta ray foraging optimization algorithm for shape optimization of complex CCG-ball curves," *Knowl.-Based Syst.*, vol. 240, Mar. 2022, Art. no. 108071.
[28] W. Zhao, Z. Zhang, and L. Wang, "Manta ray foraging optimization: An effective bio-inspired optimizer for engineering applications," *Eng. Appl. Artif. Intell.*, vol. 87, Jan. 2020, Art. no. 103300.
[29] J. Lepine, V. Rouillard, and M. Sek, "On the use of machine learning to detect shocks in road vehicle vibration signals," *Packag. Technol. Sci.*, vol. 30, no. 8, pp. 387–398, Aug. 2017.

FUJING XU received the B.S. and Ph.D. degrees from the North University of China, in 2011 and 2016, respectively. He is currently an Associate Professor with Shanxi University. His research interests include dynamic measurement and control and intelligent instrument and intelligent Internet of Things technology.

TINGWEI JIA received the B.E. degree from the North China University of Science and Technology, Tangshan, China, in 2020. She is currently pursuing the master's degree with the School of Automation and Software Engineering, Shanxi University, Taiyuan. Her major research interests include intelligent instrument and dynamic test.

RUIRUI JING received the B.E. degree from Shanxi University, Taiyuan, in 2020, where she is currently pursuing the master's degree with the School of Automation and Software Engineering. Her research interests include safety evaluation technology of coal-bed methane storage and transportation in complex environment.